Investigation of energy-release mechanisms in a turbulent current sheet

A. T. Altyntsev, V. I. Krasov, N. V. Lebedev, and V. L. Papernyĭ

Siberian Inst. of Terrestrial Magnetism, Ionosphere, and Radiowave Propagation, Siberian Div., USSR Academy of Sciences

(Submitted 24 August 1987)
Zh. Eksp. Teor. Fiz. **94**, 75–88 (September 1988)

The magnetic-structure evolution and the spatial energy distribution of the electrons of a current sheet in a theta-pinch plasma are investigated. It is shown that in the initial stage of the reconnection the energy release is via uniform ohmic current dissipation causing a "flareup" heating of the electrons. The evolution of the reconnection leads to formation of magnetic islands, i.e., to current concentration and to current fibers with dense highly conducting plasma, where the ohmic dissipation is "turned off." The energy release is localized in the islands, into which the field energy flows in with the plasma, and in which it is released via hydrodynamic motions into the ionic component. High-energy electrons are observed in the vicinity of the *O* point during this stage.

1. INTRODUCTION

Current sheets between plasma regions with antiparallel magnetic fields are the object of extensive experimental and theoretical investigations (see, e.g., Kadomtsev's review paper[1]). The main reason is that the magnetic-field energy accumulation and release in the current sheets play an important role for a large number of astrophysical objects, such as solar flares,[2] the magnetosphere tail,[3] and others. The anomalous heat transfer mechanisms in tokomaks[4] are also attributed to magnetic islands produced in the current sheet of a toroidal plasma column. Finally, dissipative processes that take place in the current sheet determine the dynamics of formation of plasma configuration of the "compact torus" type in pinches with inverted fields.[5]

The magnetic structure of laboratory current sheets has been the subject of many studies,[6–9] which have shown that the evolution of the force-line reconnection process leads to formation of magnetic islands in the sheet. Less investigated is the conversion of the magnetic-field energy into the current-sheet plasma energy. One of the considered mechanisms of this process is Joule heating of the electron via current dissipation in the anomalous (turbulent) resistance. Some results of the study of this mechanism are reported in Refs. 10 and 11. Indications of another heat-release mechanism, connected with restructuring of the mangetic-structure topology of the current sheet, and leading to ion acceleration and heating, were obtained in Ref. 12. The aim of the present paper is to establish, by a detailed study of the dynamics of the sheet's magnetic structure and of the parameters of the electronic component, a connection between various heat-release mechanisms and the reconnection process, with principal attention paid to the electronic energy-release channel.

2. APPARATUS AND DIAGNOSTIC METHODS

1. The experiments were performed with the "UN-Feniks" facility. The plasma (hydrogen) was produced in cylindrical glass vessel 100 cm long and 18 cm in diameter, placed in a quasistationary magnetic field $B_0 \approx 300$–450 G directed along the vessel axis. The initial density ($n_0 = 10^{12}$–10^{13} cm^{-3}) was monitored by a triple Langmuir probe. Plasma with a frozen-in magnetic field $\mathbf{B}_0$ was compressed by the field $\tilde{\mathbf{B}}$ of a shock loop of width $L = 30$ cm and encircling the vessel. The field of the loop, of amplitude $\tilde{B}_{\max} = 1400$ G and half-period 10 μs, was antiparallel to the field $\mathbf{B}_0$.

The magnetic structure of the sheet was investigated with a system of six radially spaced magnetic probes. The time resolution of the system was determined by the accuracy of the temporal tie-in of the different measurement channels, and amounted to ~ 10 ns. The probes measured the field component B_z in the direction of apparatus axis, along which the probes were spaced $\Delta z = 2$ cm apart. Thus, a sequence of "shots" yielded the spatial distribution of the component $B_z(r, z)$ in the volume under the shock loop, and the value of B_z in each probe position was averaged over three "shots." The measurements have shown that the dynamics of the magnetic structure is determined by the initial plasma parameters n_0 and B_0, therefore their values in each regime were maintained constant within the limits of experimental accuracy ($\sim 10\%$). Since separate measurements have confirmed the axial symmetry of the magnetic structure, the magnetic flux isolines

$$\Phi(r, z) \equiv \int_0^r B_z(\rho, z)\,\rho\,d\rho = \text{const}$$

(drawn in accordance with the $B_z(r, z)$ distribution) coincide with the magnetic-field force lines. From the measured distribution of the axial component $B_z(r, z)$ of the field we calculated also the radial component of the null line $B_r(r_0, z) = -(1/r_0)(\partial\Phi/\partial z)_{r_0}$ ($B_z(r_0, z) = 0$).

2. The energy parameters of the electron component of the plasma were investigated by analyzing, with the aid of absorbers, the x-ray bremsstrahlung from a special target placed in the plasma. The plasma parameters were chosen in this case so as to reduce to a minimum the perturbation of the magnetic structure of the sheet by the target.

The target was a tantalum-foil wedge 60 mm long, with face widths 5 mm and an angle $\alpha \approx 20°$ between them. The target in one run was parallel to the apparatus axis and at a radius $r = 5$ cm, and in the other it was inclined 60° to the axis (see Fig. 1b). The x rays from the target were recorded with a pin-hole camera. The detector was a microchannel plate (MCP) behind which a luminescent screen was placed. The image was formed on the MCP surface by two holes (1

 0038-5646/88/091777-08$04.00

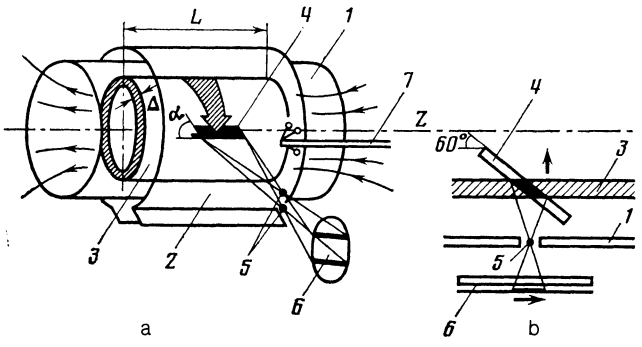

FIG. 1. Diagram of experimental setup, with the target oriented along the apparatus axis (a) and at an angle to the axis b): 1—evacuated vessel, 2—shock loop, 3—current sheet, 4—target, 5—pin-hole camera, 6—image recorder, 7—magnetic probes. The arrows indicate the electric current directions in Fig. a and the direction of motion of the current sheet and of the image of the radiating region of the target in Fig. b.

mm diam) covered by absorbers that separated different regions of the spectrum. The use of an MCP detector insensitive to visible light made it possible to employ transparent polystyrene films of thickness 2 and 4 μm and also of 1 and 2 μm, thereby substantially increasing the detector sensitivity in the ultrasoft-radiation region $\lesssim 0.5$ keV. The spatial resolution of the pin-hole camera on the target surface was determined by the geometry and equaled ~ 2 mm. The instant of switching-on the detector and the exposure duration were set by applying to the MCP electrodes, at the required instant, a rectangular supply voltage pulse of appropriate duration; the pulse amplitude determined the gain of the plate. An electron source placed directly inside the apparatus was used to calibrate the absolute sensitivity of the entire recording channel under the experimental conditions. The construction and the parameters of the pin-hole camera are described in Ref. 13.

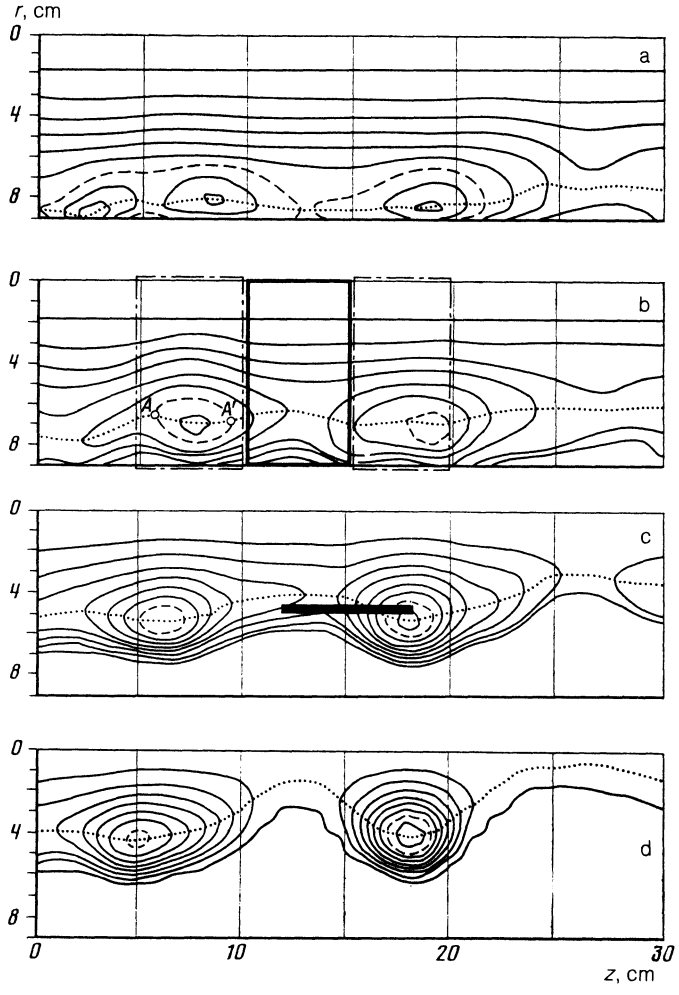

FIG. 2. Maps of magnetic-field force lines at the instants of time: 60 ns (a), 100 ns (b); 300 ns (c) and 360 ns (d). The strip shows the target location.

3. MAGNETIC STRUCTURE OF CURRENT SHEET

The evolution of the magnetic structure of the sheet was investigated by plotting, at various instants of time, maps of the magnetic-flux isolines $\Phi(r, z) = \text{const}$ in the plasma under the shock loop. The maps were plotted in the (r, z) plane, bounded in radius by the plasma volume axis ($r = 0$) and by the loop cross section ($r = 9$ cm), and limited along z by the boundaries of the shock turn ($z = 0.30$ cm). The isoline were spaced $\Delta\Phi = 10^3$ G·cm^2 apart and were bounded by the separatrix $\Phi(r, z) = 0$. In view of the boundary condition $\Phi(0, z) = 0$ on the system axis, the isolines can be identified with equal values of Φ plotted at various instants of time; each force line is thus "tagged" on the different maps so that its evolution can be tracked. By way of example, each dashed line on the maps of Fig. 2 corresponds to $\Phi(r, z) = 7 \cdot 10^3$ G·cm^2. Magnetic measurements have shown that a cylindrical current sheet of thickness $\Delta \approx 2$–3 cm and width close to that of the shock turn is formed in the plasma and moves in a radial direction towards the axis of the plasma column. The current-sheet formation is simultaneously accompanied by rearrangement of its magnetic-structure topology.

During the initial stage of this process, the force lines of the field B_0 are parallel to the z axis in the entire volume, except on the periphery of the plasma column, where they are bent by perturbations that have a B_r component. The positions and levels of the perturbations on the maps plotted in various "shot" runs have a large scatter, attesting to a *random* character of the perturbations. At 40–80 ns after the appearance of the null line of the axial component of the magnetic field ($B_z(r_0, z) = 0$) on the plasma boundary, reconnection of the initial field force lines with the antiparallel lines of the shock loop is observed, i.e., formation of closed magnetic loops—islands—out of the initial perturbations (see Fig. 2a). The longitudinal dimension λ of the islands (the distance between neighboring X-type singular points) satisfies the relation $\lambda > 2\pi\Delta$, and the scatter of their positions and dimensions, obtained in different shot runs, decreases greatly.

The structure of the sheet acquires thus in the course of island formation a *predetermined* character, and this serves as the experimental justification for the described procedure of mapping the force lines. This question is discussed by the authors in detail in Ref. 14.

The subsequent dynamics of the process is illustrated by Fig. 3, from which it is seen that the process can be arbitrarily divided into two stages. During the first, lasting 80–100 ns after the onset of the null line, a relatively rapid growth of the magnetic field contained in the islands is observed (see

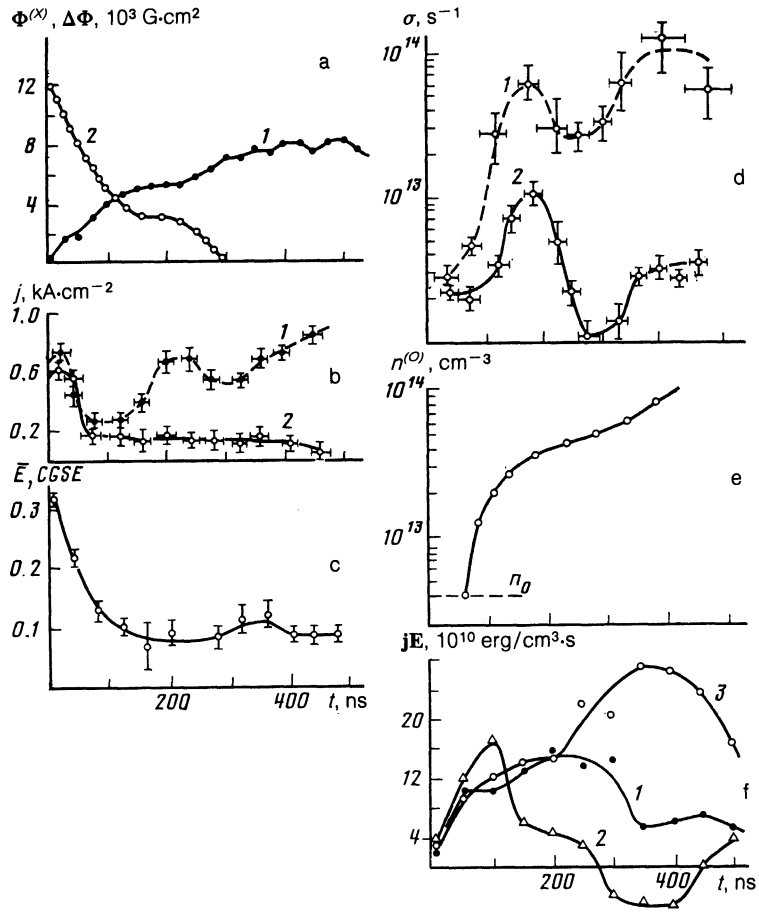

FIG. 3. Dynamics of the variation of the characteristics of the magnetic structure of the current sheet: a—of the magnetic flux ($\Delta\Phi$) trapped in an island (1) and of the non-reconnected flux at $z = 13$ cm (2); b—of the current density at the O point for $z = 6$ cm (1) and at the X point for $z = 13$ cm (2); c—of the electric field averaged along the null line; d—of the conductivity in the vicinities of the O point (1) and of the X point (2); e—of the density in the island; f—of the specific energy-release power, averaged over the plasma-column cross section, between the planes $z = 5$ and 10 cm (1), $z = 10$ and 15 cm (2), and $z = 15$ and 20 cm (3).

Fig. 3a). The time and space scales of island formation allow us to regard this stage as a development of a Thiring instability of the current sheet, which leads to spontaneous formation, out of the random initial perturbation, of a regular reconnected structure in the form of a chain of magnetic islands corresponding to current-concentration regions–current fibers.[14] Towards the end of the initial stage $B_r(r_0, z)$ reaches values $(0.2–0.3)B_b$ (B_b is the value of B_z on the boundary of the sheet, and an appreciable fraction of the initial magnetic field turns out to be enclosed in the produced islands. This is followed by observation of a comparatively slow growth of the flux enclosed in the islands, in view of the further decrease (to zero by the instant $t = 300$ ns) of the reconnected magnetic flux (curve 2, Fig. 3a).

The evolution of the reconnection indicates further concentration of the current fibers. This process is illustrated by Fig. 3b, from which it is seen that when the null line appears the current density decreases rapidly and uniformly along the sheet, after which the current density $j^{(O)}$ in the vicinity of the O point increases, while the current density $j^{(X)}$ in the vicinity of the X point decreases slowly. Thus, over long times, almost all the current is concentrated in the current fibers into which the extended current sheet breaks up.

The rate of change of the magnetic flux in the island-formation process is characterized by the resultant azimuthal electric field E_φ. For an annular loop of radius $r_0(z, t)$ passing over the current sheet in the vicinity of the null line we get, assuming axial symmetry,

$$E_\varphi(r_0^{(1)}, z) \approx \frac{1}{cr_0^{(1)}} \frac{\Delta\Phi}{\Delta t}, \tag{1}$$

where

$$\Delta\Phi = \Phi(r_0^{(2)}, z) - \Phi(r_0^{(1)}, z), \quad r_0^{(1,2)} = r_0(t^{(1,2)}), \quad \Delta t = t^{(2)} - t^{(1)}. \tag{a}$$

The time variation of the field $\overline{E}$ averaged along the null line and characterizing the average rate of ohmic dissipation in the sheet is shown in Fig. 3c. It is seen from this figure that towards the end of the initial stage the value of $\overline{E}$ decreases substantially compared with the initial value, indicating that the dissipation rate has decreased by that instant.

The values of the field in the vicinity of the singular points X and O (where $B_r \approx B_z \approx 0$), calculated from Eq. (1), and also the corresponding values obtained above for the current density (see Fig. 3b) have made it possible to estimate the local conductivity of the plasma in the vicinities of the singular points. We used in the estimate the equation $j = \sigma E$, with values of j and E averaged over these vicinities. The time dependences of the values of $\sigma^{(X)}$ and $\sigma^{(O)}$ obtained in this manner are shown in Fig. 3d, from which it can be seen that at the start of the reconnection process the conductivity is weakly inhomogeneous along the sheet and its value is low. Towards the end of the first stage the conductiv-

ity in the sheet increases rapidly, especially in the islands, where its value (at $t > 150$ ns) exceeds by more than an order the value at the X point. Thus, by the end of the initial stage the conductivity distribution in the sheet becomes strongly inhomogeneous, and the dynamics of its variation in the vicinity of the X and O points begins next to differ greatly. The time dependence of the conductivity in the vicinity of the X point has a clearly pronounced oscillatory character (curve 2 of Fig. 3d). The conductivity in the vicinity of the O point remains at all times substantially higher than at the X point, and executes similar (albeit less pronounced) oscillations.

Island formation causes also strong bunching of the plasma density in the sheet. The closed field force lines produced at the start of the reconnection process contract rapidly towards the center of the island (see Figs. 2a and 2b), with characteristic times $\Delta t \approx 40$–60 ns. The spatial scale l_d of plasma diffusion during that time, estimated from the initial, minimial conductivity $\sigma_0 \approx 2 \cdot 10^{12}$ s^{-1} ($l_d \approx (\Delta t c^2/4\pi\sigma_0)^{1/2} \approx 0.7$ cm), is small compared with the decrease of the island's length ~ 7 cm. This means that pinching of the corresponding current fiber, i.e., "rake-up" of the plasma into the island and a rapid increase of the density in the vicinity of the O point. Let us analyze this effect, estimating the density $n^{(0)}(t)$ in a current fiber bounded by the dashed force line of Fig. 2. Assuming that by the instant of formation of the closed line ($t \approx 60$ ns) the plasma density is close to the initial value, $n^{(0)}(t) \approx n_0$, we obtain a rapid density growth as a result of the decrease of the fiber cross-section area ($t \lesssim 140$ ns, see Fig. 3e). The growth of the density is then slowed down and is due subsequently to the radial motion of the current fiber towards the axis of the plasma column.

A fast growth of the plasma density in the islands towards the end of the initial stage, with account taken of the slow variation, during the same interval, of the radial profile of the component B_z (i.e., of the magnetic pressure), is possible if it is assumed that the plasma cools off during that time. We estimate the plasma temperature in the island during the succeeding stage of slow structure evolution by assuming that the plasma is in hydrodynamic equilibrium. At the points A and A' on the null line (see Fig. 2b), where $|B_r|$ reaches a maximum, the condition that the plasma and magnetic-field pressures be in balance yields the estimate $T_e + T_i \approx 100$–200 eV.

We consider next the energy-release dynamics in various regions of the current sheet. From the experimental values of $B_z(r, z, t)$ we calculated the values of the specific power $\mathbf{j}\cdot\mathbf{E}$ of this process, averaged over cylindrical plasma volumes that enclose the O-point vicinities (the boundaries of the intersections of these volumes with the (r, z) plane are shown dashed in Fig. 2b), and over the corresponding volume enclosing the vicinity of the X point (the boundary of the volume cross section is shown by a thick line). It is convenient to use for the calculations the integral relation

$$\overline{\mathbf{jE}} \approx \frac{1}{V}\left[-\frac{1}{8\pi}\frac{d}{dt}\int B^2\, dV - \frac{c}{4\pi}\oint_S [\mathbf{EB}]\, ds\right], \qquad (2)$$

which leads to higher accuracy than direct calculation of the local value of $\mathbf{j}\cdot\mathbf{E}$. Here $V = \pi R_0^2 \Delta z \approx 10^3$ cm^3 is the averaging volume, $\Delta z = 5$ cm and $R_0 = 9$ cm are the width and radius of the volume, and S is the area bounding the volume.

Relation (2) determines the *total* magnetic field energy released in the indicated plasma volume and in both components. It can be seen from Fig. 3f, which shows the dynamics of the variation of $\overline{\mathbf{j}\cdot\mathbf{E}}$ in the vicinities of the X and O points, that the energy release during the initial stage is practically uniform along the layer. During the next stage ($t > 140$ ns), the power released in the vicinity of the X point decreases steeply. The power level in the islands remains high, but in the right-hand island the power at $t > 240$ ns increases rapidly. Note that the isoline maps show at the same time a deformation, viz., "rounding-off" of the island (see Figs. 2c and 2d), whereby the force lines of the magnetic field with a plasma that is "frozen-in" (as shown by estimates) move from the X points towards the island center.

4. ENERGY STRUCTURE OF THE CURRENT SHEET

Analysis of x-ray bremsstrahlung by electrons on the surface of an extended target yielded the axial structure of the energy-release region of the electron component of the plasma, and permitted a study of the dynamics of the initial stage of the energy release in the layer. In the first set of experiments, devoted to the structures of the energy-containing regions, the target was parallel to the axis of the setup on a radius $r = 5$ cm. The experiments were performed at initial plasma parameters (n_0, B_0) that controlled the magnetic structure of the sheet in such a way that the null line reached the target at a time ~ 100 ns after the appearance of

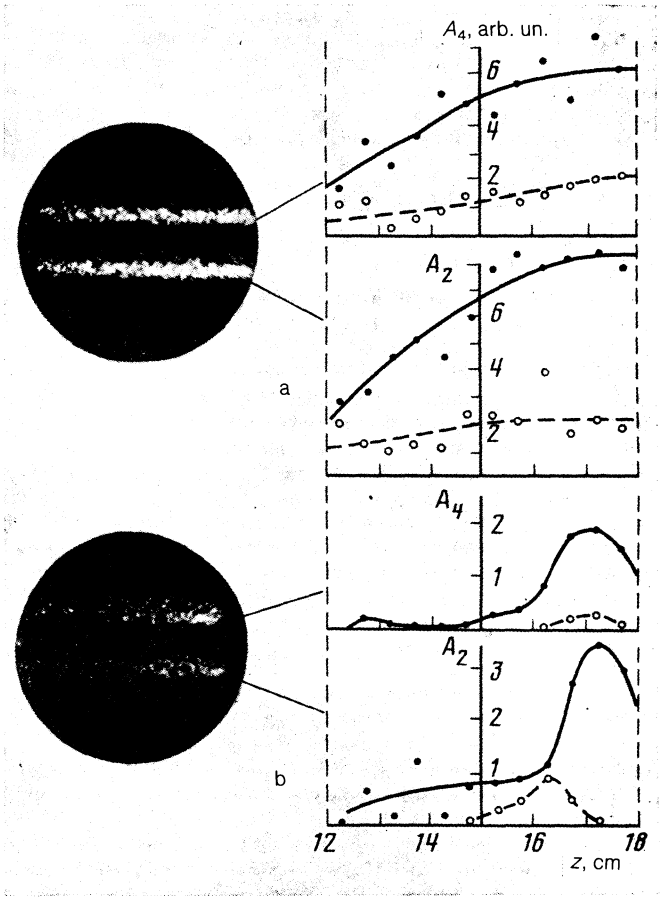

FIG. 4. Target images and longitudinal signal-level distributions on the photographs if the upper (●) and lower (○) target faces (see Fig. 1a), obtained with absorbers of thickness 4 (A_4) and 2 μm (A_2) at the instants 100 (a) and 240 ns (b). The dashed lines show the target boundaries.

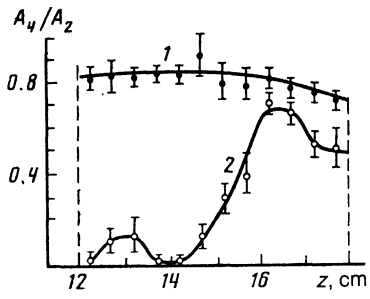

FIG. 5. Distribution, along the target, of the level ratio of the signals from the upper face of the target, obtained with different absorbers at the instants 100 ns (1) and 240 ns (2).

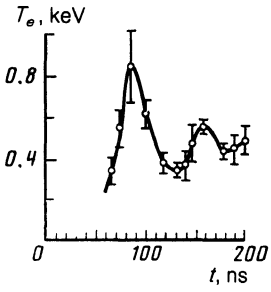

FIG. 6. Dynamics of the electron temperature during the initial energy-release stage.

a plasma column on the boundary. The measurements have shown that the target radiates only when the current sheet moves past it, and that the radiation level is not uniform along the target (see Fig. 4a). However, the level ratio of the signals passing through different absorbers, which is therefore indicative of the energy of the radiating electrons, remains almost constant (curve 1 of Fig. 5). It follows hence that the brightness modulation is due in this case to the density inhomogeneity of the radiating electrons, and the distribution of their energies along the sheet remains in this case practically uniform. Assuming that the radiation is due to thermal electrons, we obtain, from the signal ratio obtained from target photographs made with different absorbers, a temperature $T_e \approx 0.8$–1.0 keV that agrees with the earlier measurements performed with a multichannel x-ray pickup.[13] The radiation intensity dropped to below the recording threshold when the absorber was a polystyrene film 24 μm thick. This confirms the assumption that the main contribution to the radiation is made by the low-energy part of the electron spectrum with energy $\lesssim 2$ keV. An absolute calibration of the recording channel has made it possible to determine, from the measured value of T_e, the density $n_{\text{rad}} \approx (2$–$5) \cdot 10^{12}$ cm^{-3}, which turned out to be of the same order as the initial plasma density n_0. This is another confirmation of the thermal origin of the radiating electrons.

The brightness difference between the images of the upper face, oriented counter to the current (as shown in Fig. 1) and the lower one oriented along the current suggests that the electron spectrum is anisotropic, i.e., that the bulk of the electrons have a directed current velocity v_d. When the orientation of the magnetic field on the sheet boundary is reversed, so that the current direction in the sheet is also reversed, the higher-intensity radiation comes from the lower face, thus confirming the assumption made. If it is assumed that the thermal part of the electron distribution function is Maxwellian, with a shift equal to the current velocity v_d, the ratio of the signal levels from the different faces (see Fig. 4a) can be used to estimate the degree of anisotropy of the electron spectrum, i.e., the ratio of the current and thermal velocities. In our case the estimate yields $v_d/v_{T_e} \approx 0.2$–0.3. The homogeneous axial energy structure of the sheet during the initial stage of the energy release has made it possible to investigate, with the aid of the same procedure, the electron-heating dynamics. To this end, the target was oriented, in a second set of experiments, at an angle to the axis of the volume (see Fig. 1b). In this setup the radiation source at each instant of time was the local target region intersected at that instant by the current sheet. For radial motion of the sheet, this region moved over the target, producing on the image a "time scan" of the homogeneous sheet. The ratio of the signal levels on the photographs of two target images produced by x rays passing through absorbers 1 and 2 μm thick yielded the electron temperature in the sheet at each instant of time.

The measurement results are shown in Fig. 6. It can be seen that the electron temperature T_e increases rapidly (within a time $\lesssim 80$ ns which is short compared with sheet lifetime) to a maximum value $T_e \approx 1.0$ keV, after which it decreases rapidly, i.e., the initial stage of the electron heating has a "flareup" character.

To study the structures of the energy-containing regions during a later stage of the sheet evolution, when islands are formed, measurements were made with a target oriented, just as in the first run, along the apparatus axis, likewise at a radius $r = 5$ cm. The initial plasma parameters were close in this case to the conditions of Fig. 2. The null line reached the target at ~ 240 ns after the onset of the plasma column at the boundary. The images of the target faces and the image photographs obtained under these conditions are shown in Fig. 4b. It is seen from the figure that the axial distributions of signal levels obtained with different absorbers, as well as the ratios of these levels (see Fig. 5), are now distinctly inhomogeneous. This means that the distribution of the radiating-electron energy along the layer becomes, in contrast to the preceding stage, essentially inhomogeneous. Assuming that insertion of the target leaves the magnetic structure of the sheet as a whole unchanged, it can be assumed that the energetic electrons are localized at that instant in the vicinity of the O point. The electron energy decreases abruptly towards the periphery of the localization region, and the radiation level of the remaining part of the sheet turns out to be lower than the registration threshold, indicating that the electron component has a low energy content in that region. The large level ratio of the signals from target faces oriented parallel and antiparallel to the current (Fig. 4b) is evidence of an increased anisotropy of the electron spectrum, i.e., of the ratio of the directed and thermal electron velocities. Assuming therefore that the form of the spectrum of the radiating electrons can also change during this stage, we estimate their energy and density at the maximum-radiation point ($z = 17$ cm) for two models of the spectrum, isotropic Maxwellian and a monoenergetic beam. The estimates obtained ($T_e \approx 0.1$ keV, $n_{\text{rad}} \approx 10^{14}$ cm^{-3} in the first case and $\varepsilon_0 \approx 1.0$ keV, $n_{\text{rad}} \approx 10^{12}$ cm^{-3} in the second) do not contradict the preceding results and suggest a possibility of realizing either of the two radiating-electron model spectra.

5. DISCUSSION OF RESULTS

The measurement results suggest the following picture of the magnetic-field energy dissipation in the current sheet. The initial stage ($t \lesssim 100$ ns) consists of a rapid dissipation, uniform along the sheet, of the current by the anomalous resistance, leading to an intense Joule heating of the electrons up to a temperature $T_e \approx 1$ keV. The results of earlier probe measurements,[15] as well as the value $v_d/v_{T_e} \approx 0.2$–0.3 obtained from x-ray measurement data, indicate that the anomalous resistance is due to the development, in the sheet, of a small-scale (ion-sound) turbulence. It was shown earlier[15] that a second energy-release channel can also be realized during this stage in the current-sheet plasma, viz., acceleration, observed using a multichannel x-ray pickup, of a small fraction ($n_{acc}/n_0 \lesssim 10^{-2}$) of the electrons from the "tail" of the distribution, to a maximum energy $\varepsilon_{acc} \approx (15$–$20)T_e$ (10–12 keV). The energy $(n_{\bar{\varepsilon}})_{acc}$ of the accelerated particles, however, is a small fraction of the total energy $(n_{\bar{\varepsilon}})_{acc} \lesssim 0.1 n_0 T_e$ contained in the plasma. The main energy-release channel during this stage remains therefore the Joule heating of the thermal electrons.

We analyze the dynamics of the initial stage of the heating, using the energy balance equation

$$n\frac{dT_e}{dt} \approx \frac{j^2}{\sigma} - \varkappa_{eff}\frac{T}{(L/2)^2}, \qquad (3)$$

where the first term in the right-hand side describes the Joule heating of the electrons as a result of the current dissipation by the anomalous resistance, while the second term describes the longitudinal cooling due to anomalous heat conduction, which is the principal loss mechanism in this case. The reconnection process leads rapidly to the onset of a transverse field component $B_r(r_0, z)$ on the null line, and as a result the electrons can become magnetized along the sheet. In estimates of this effect, the width of the barrier can be assumed to be the axial dimension of the island, and the height can be determined from the average value $\bar{B}_r$ of the field at this dimension. During the initial reconnection stage, when B_r and σ_{eff} are small (i.e., the effective collision time $\tau_{eff} = m\sigma_{eff}/ne^2$ is short), the electrons remain non-magnetized along the transverse field $\omega_{B_r}\tau_{eff} \lesssim 1$ ($\omega_{B_r} = e\bar{B}_r/m_e c$), and only towards the end of this stage does the growth of B_r and of τ_{eff} (see Fig. 4d) cause the parameter $\omega_{B_r}\tau_{eff}$ to reach values ~ 2–3. The thermal conductivity in Eq. (3) retains therefore during almost the entire initial stage, just as in the case of a homogeneous sheet, the form

$$\varkappa_{eff} \approx \varkappa^* \equiv 3.6 T_e \sigma_{eff}/e^2.$$

The dynamics of the initial electron-heating stage, while T_e is still low enough and, as shown by estimates, the thermal losses can be neglected, is determined by the first term in the right-hand side of (3). The value of j in this term is determined by the magnetic-field configuration which is controlled by an external source—the shock loop. The rapid compression of the sheet by the loop field, which leads to high values of j, causes an intense Joule heating of the electrons, and this process is so rapid that the system "jumps through" the equilibrium state in which the electron temperature T_{eq} is determined by the vanishing of the right-hand side of (3):

$$T_{eq} \approx 0.3e(L/2)E \approx 200 \text{ eV} \qquad (4)$$

and can reach in a time ~ 10–20 ns a value $T_e \approx 1$ keV. The rapid growth of T_e and of the conductivity in the sheet leads to higher thermal losses, so that at $T_e > T_{eq}$ the second term of (3) becomes predominant and the sheet cools off. The "flareup" character of the initial stage of the energy release in the sheet is indeed observed in experiment (see Fig. 6). The high initial-stage longitudinal electronic thermal conductivity, due to the high values of T_e and σ_{eff} and to the low value of the parameter $\omega_{B_r}\tau_{eff}$ cause the axial energy structure of the sheet to remain practically uniform during this stage (see Fig. 5).

The abrupt increase of the conductivity in the layer towards the end of the initial stage attests to a lowering of the level of the conductivity-controlling ion-sound turbulence. The higher conductivity in the island is due arparently to the aforementioned rapid growth of the plasma density ($\sigma_{eff} \propto n/\nu_{eff}(W) \propto n^{1/2}$, Ref. 15). The decrease of the turbulence level can, in turn, be attributed to the decrease of v_d/v_{T_e} at the end of the initial stage. In fact, both the increase of $n_e(t)$ (see Fig. 3e) and the decrease of $j(t)$ (see Fig. 3b) lead to an abrupt decrease of $v_d = j/en$, whereas $v_{T_e} \propto T_e^{1/2}$ decreases relatively weakly during the initial stage. Estimating these quantities for the initial stage ($t \approx 80$ ns, $T_e \approx 1.0$ keV, $n \approx n_0 \approx 4\cdot 10^{12}$ cm^{-3}, $j \approx 4\cdot 10^2$ A/cm^2) we have ($t \approx 120$ ns, $T_e \approx 0.2$ keV, $j \approx 2\cdot 10^2$ A/cm^2, $n \approx 3\cdot 10^{13}$ cm^{-3}) $v_d/v_{T_e} \approx 0.02$.

A characteristic feature of the initial energy release stage is the high specific ohmic-dissipation power j^2/σ in the vicinity of the null line. In fact, from Figs. 4b and 3d we get $j^2/\sigma \approx 7\cdot 10^{11}$ erg/cm^3·s at $t \approx 40$ ns, much higher than the total specific power release $\overline{\mathbf{j}\cdot\mathbf{E}} \approx 1.0\cdot 10^{11}$ erg/cm^3·s averaged over the plasma-column cross section (see Fig. 3f). Consequently, the initial stage of the reconnection process, which is due to development of Thiring instability, takes place against the background of high-power homogeneous ohmic current dissipation that determines the energetics of the sheet during that period. The contribution to the energy release from mechanisms connected with layer-topology restructuring accompanied by hydrodynamic plasma motion turns out to be small during this stage. This is apparently due due to the small volume of the plasma set in motion from the vicinity of the null line. Note the decisive role of the current-driven small-scale (ion-sound turbulence during the initial stage of sheet evolution, where it controls both the rate of rearrangement of the magnetic structure[14] and the dynamics of the energy-release processes.

Let us consider the features of the succeeding stage of this process. The described "flareup" dynamics of the initial stage can cause the subsequent energy release in the layer to become oscillatory, as shown in Ref. 11. This requires that Joule heating remain the principal energy-release mechanism, and that the longitudinal heat conduction remain the principal loss mechanism. From Fig. 3d, which shows the conductivity dynamics (a parameter indicative of the Joule dissipation power), it is clear that the dissipation oscillations are indeed similar to those described in Ref. 11. This effect is clearly seen in the sheet region between the islands, where an X point exists for 300 ns and the heat removal is along the open force lines, just as in the case of the uniform sheet dur-

ing the initial stage (see curve 2 of Fig. 3d). In the island, however, where the heat removal is suppressed by the magnetic "barrier" due to the electron magnetization along the transverse field B_r ($\omega_{B_e}\tau_{\text{eff}} \gtrsim 10$ for $t > 200$ ns) the oscillatory character of the conductivity is weakly pronounced (curve 1 of Fig. 3d).

It appears thus that in the vicinity of the X point the Joule heating still remains the principal energy-release mechanism, but its power is substantially lower than in the initial "flareup" stage. Indeed, from Figs. 2b and 2d we get for $t > 250$ ns $(j^2/\sigma)^{(X)} \approx 3\cdot 10^{10}$ erg/cm$^3\cdot$s, which is lower by more than an order than the value during the initial stage. The reason is that the sheet, as it oscillates, relaxes to a state of equilibrium energy release (described by Eq. (3) with zero left-hand side), in which the dissipation rate is controlled by the slow heat removal along the extended current sheet.

The character of the energy release is different in the islands. The rapid growth of the conductivity in the viciniy of the O point leads to an abrupt decrease, by almost two orders, of the ohmic dissipation power: $(j^2/\sigma)^{(O)} \approx (1\text{–}6)\cdot 10^{10}$ erg/cm$^3\cdot$s (at 300 ns $\lesssim t \lesssim$ 500 ns) according to the data of Figs. 3b and 3d. The *total* magnetic-field specific power release in the plasma, $(\overline{\mathbf{j}\cdot\mathbf{E}})^{(O)} \approx 2\cdot 10^{11}$ erg/cm$^3\cdot$s (see curve 3 of Fig. 3f) turns out to be substantially higher than $(j^2/\sigma)^{(O)}$. It follows hence that, first, the energy release previously localized in the vicinity of the null line is now in the entire island (i.e., in the entire volume of the corresponding current fiber). Second, the abrupt decrease of the contribution made to the total energy release by the ohmic dissipation that leads to the electron heating suggests that the main channel of this energy-release stage is connected with the ion component. It is seen from Figs. 2c and 2d that in this stage there is also a deformation of the magnetic-island structure, whereby the force lines of the field with the frozen-in plasma move towards the center of the island. As shown by analysis of Eq. (2), this hydrodynamic motion of the plasma leads to the onset of field-energy fluxes in the same direction, and this in turn causes the energy-release power to decrease in the vicinity of the X point and to increase in the vicinity of the O point. The data shown in Fig. 3f illustrate this effect, which is particularly pronounced in the first island (see curve 3), where the force lines are strongly deformed during the evolution of the structure. This result confirms the assumption made above concerning the character of the later stage of the heat release in the islands.

The observation of a region of energetic electrons during the later stage can be attributed to two causes. First, these may be thermal electrons, trapped in an island, with a temperature lower and with a density higher than in the initial stage. The small heat removal from the island permits the electrons to retain here a much higher temperature than in the surrounding cold plasma. Confirming this assumption is the fact that the temperature and density of the "hot" electrons, obtained from x-ray measurements, are close to the estimates obtained from the hydrodynamic-equilibrium condition. Second, one cannot exclude also another source of energetic electrons, resulting from acceleration of a small fraction ($n_{\text{acc}} \lesssim 10^{-2} n_0$) of superthermal electrons from the distribution "tail." Acceleration in a sheet with an advanced reconnected structure can take place in the vicinities of the singular points, where the transverse magnetic field is weak; this is likewise in agreement with the assumed localization of the energetic electrons in the vicinity of the O point, which serves as a trap for them. The feasibility of an accelerating mechanism is attested by the high level of the conductivity in the island.

CONCLUSION

We have investigated the evolution of the magnetic structure of a current sheet, and also the dynamics of the energy contained in the electron component, and the distribution of the electron energy along the sheet. Analysis of our present and earlier experimental data leads to the following conclusions:

1. The principal mechanism of the initial energy-release stage is ohmic dissipation, uniform along the layer and localized in the vicinity of the null line, of the current in the anomalous resistance. The reconnection makes a small contribution to the energetics of the processes during this stage.

2. Dissipation causes an intense "flareup" heating of the electrons, due to rapid compression of the sheet by the field of the extenral field (of the shock loop in this case) and to the competition between the Joule-heating and longitudinal-heat-removal mechanisms; the axial structure of the sheet energy remains uniform in this case.

3. Reconnection produces in the layer current fibers with a highly conducting, dense, and cold (compared with the initial stage) plasma, in which the ohmic dissipation is "turned off."

4. As a result, the character of the succeeding stage of the energy release is substantially altered. In the vicinity of the X point it consists, as before, of ohmic dissipation of the current; the main energy release is localized in the islands. The field energy flows into the islands with the plasma from the vicinity of the X point, and is released to the ionic component via the hydrodynamic motions of the plasma.

5. The energy structure of the layer becomes essentially inhomogeneous: relatively high energy electrons are localized in the vicinity of the O point, while the energy-content level of the electrons in the neighboring regions of the sheet is substantially lower.

We have thus confirmed the roles of the small-scale (ion-sound) turbulence and of the reconnection-induced rearrangement of the large-scale magnetic structure of the layer in various regions and in various stages of the energy release. The turbulence controls the initial stage of the energy release, which proceeds via the electronic channel. The reconnection and the concommitant hydrodynamic processes determine the principal channel of the next stage of energy-release in the island via the ion component.

[1] B. B. Kadomtsev, Usp. Fiz. Nauk **151**, 3 (1987) [Rep. Prog. Phys. **50**, 115 (February 1978)].
[2] S. I. Syovatskiĭ, Vestn. AN SSSR, No. 10, 33 (1977).
[3] L. M. Zelenyi, Itogi Nauki i Tekhn., Ser. Issled. Kosm. Prostr. (Outer Space Studies), VINITI, Vol. 24, p. 68 (1986).
[4] S. V. Mirnov, Physical Process in Tokamak Plasma [in Russian], Energoatomizdat, 1985, Chap. 6.
[5] R. Kh. Kurtmullaev, A. I. Malyutin, and V. N. Semenov, Itogi Nauki is Tekhn. Ser. Fiz. Plazmy (Plasma Physics), VINITI, Vol. 9, p. 80 (1985).

[6]A. T. Altyntsev and V. I. Krasov, Zh. Tekh. Fiz. **44**, 2629 (1974) [Sov. Phys. Tech. Phys. **19**, 1639 (1975)].
[7]A. G. Frank, Tr. FIAN **160**, 93 (1985).
[8]A. Sevilliano and F. L. Ribe, Phys. Fluids **28**, 3142 (1985).
[9]J. N. Irby, J. F. Drake, and H. R. Griem, Phys. Rev. Lett. **42**, 228 (1979).
[10]A. T. Altyntsev, V. I. Krasov, N. V. Lebedev, *et al.*, Pis'ma Zh. Eksp. Teor. Fiz. **33**, 518 (1981) [JETP Lett. **33**, 502 (1981)].
[11]A. T. Altyntsev, V. M. Bardakov, and V. I. Krasov, Zh. Eksp. Teor. Fiz. **81**, 901 (1981) [Sov. Phys. JETP **54**, 480 (1981)].
[12]S. Yu. Bogdanov, V. S. Markov, and L. G. Frank, Pis'ma Zh. Eksp. Teor. Fiz. **35**, 232 (1982) [JETP Lett. **35**, 290 (1982)].
[13]A. T. Altyntsev, V. I. Krasov, N. V. Lebedev, *et al.*, Fiz. Plazmy **8**, 115 (1982) [Sov. J. Plasma Phys. **8**, 65 (1982)].
[14]A. T. Altyntsev, V. I. Krasov, N. V. Lebedev, *et al.*, Pis'ma Zh. Eksp. Teor. Fiz. **45**, 17 (1987) [JETP Lett. **45**, 20 (1987)].
[15]A. T. Altyntsev and V. I. Krasov, Fiz. Plazmy **5**, 996 (1979) [Sov. J. Plasma Phys. **5**, 556 (1979)].

Translated by J. G. Adashko